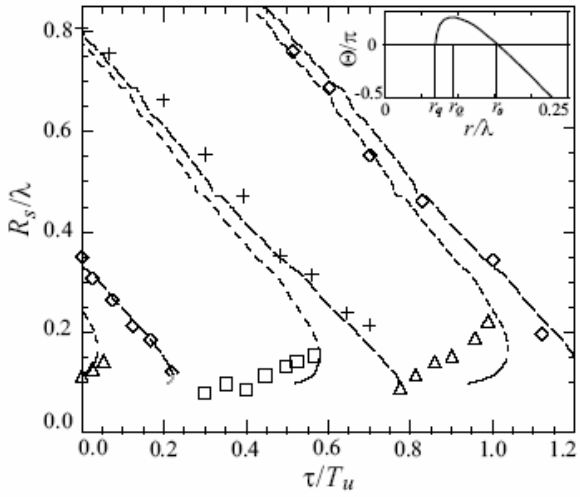


Figure 4: Attractor radius $R_s$ for different delay times $\tau$: diamonds and crosses, epicycloidal attractors with negative ($A = -0.030$ mW/cm$^2$) and positive pulse ($A = 0.051$ mW/cm$^2$); triangles and squares, hypocycloidal attractors with positive ($A = 0.041$ mW/cm$^2$) and negative pulse ($A = -0.031$ mW/cm$^2$), where $I_0 = 0.061$ mW/cm$^2$. Solid and short-dashed curves are prediction of $R_s(\tau)$ from equations (1) and (2) for stable and unstable hypocycloidal attractors, resp, with $h_n = 0.215 \pm 0.003$ mm, $\psi_n = 4.00 \pm 0.11$ rad for negative, and $h_p = 0.328 \pm 0.005$ mm, $\psi_p = 0.91 \pm 0.07$ rad for positive pulse. Similarly, long-dashed and dotted curves are prediction of $R_s(\tau)$ for stable and unstable epicycloidal attractors, resp. Insert: function $\Theta(r)$ specifying the experimentally observed shape of the spiral wave front. $\Theta(r)$ increases with $r$ in the vicinity of the core radius $r_q$, reaches a maximum at $r = r_Q$, and becomes negative for $r > r_0$.

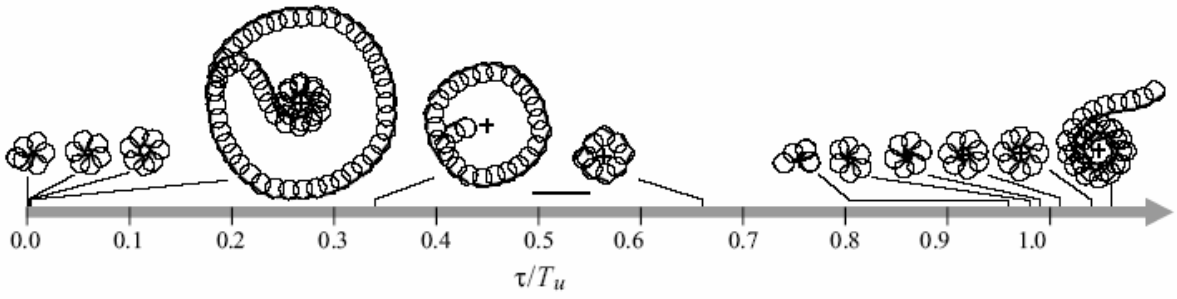


Figure 5: Simulation of epi- and hypocycloidal attractors computed from equations (3) and (4) for positive pulse ($A = 0.0035$, duration $= 12.19T_u$) under variation of $\tau$. The measuring point (crosses) was initially placed close to the unperturbed spiral core. Thick segments correspond to the application of the light pulses. Scale bar: 20 s.u.

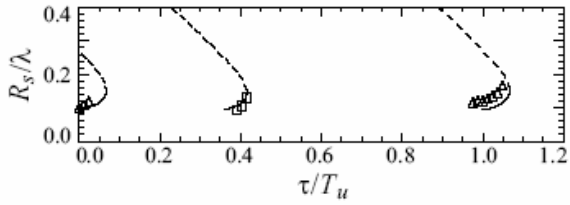


Figure 6: Attractor radius $R_s$ for different $\tau$: triangles, attractors with positive pulse; squares, attractors with negative pulse ($A = -0.0020$, duration $= 12.19T_u$), with background value $\phi_0 = 0.01$. Solid and dashed curves: $R_s(\tau)$ for stable and unstable solutions, resp, computed from equation (2) with: $h_n = 0.097\lambda$, $\psi_n = 5.026$ for a negative pulse; $h_p = 0.128\lambda$, $\psi_p = 0.848$ for a positive pulse.

$$\frac{\tau}{T_u} = \frac{\Theta(R_s) - \arccos(h/(2R_s)) - \psi}{2\pi} + m, \tag{1}$$

$$\frac{\tau}{T_u} = \frac{\Theta(R_s) + \arccos(h/(2R_s)) - \psi}{2\pi} + m. \tag{2}$$

Here $m$ is a positive integer. The function $\Theta(r)$ (see insert of Fig. 4) and the values $h$ and $\psi$ are measured quantities (cf. [17]). The size of the resonance orbit can then be predicted at any time delay $\tau$ by substituting these data into equations (1) and (2). Linear stability analysis shows that equation (1) describes stable orbits and equation (2) unstable ones [16]. The computed results are shown in Fig. 4, where each branch of the dependency $R_s(\tau)$ was obtained for a fixed value of $m$.

In this figure there are mostly long-dashed branches and mostly short-dashed branches. The mostly short-dashed curves were computed from equation (2), with a positive sign in front of $\arccos(h/(2R_s))$. Since the change of slope of the $\Theta(r)$ curve in the interval from $r_q$ to $r_0$ implies a switching of stability [16], there is an unstable portion of these curves (short-dashed) and a stable one (solid). Consider the shortest branch close to the ordinate of Fig. 4 ($\tau/T_u \leq 0.05$). Our experimental results suggest that with positive pulses there exist only hypocycloidal attractors in this interval, whereas epicycloidal ones will not be stable. In a similar manner, the existence of other sets of hypocycloidal resonance attractors observed in experiments (all squares and triangles in Fig. 4) can be explained with other branches computed according to equation (2). Note that there are very small unstable branches (e.g., dotted arc-shaped segment at $\tau/T_u \approx 0.2$) at the lower end of each stable branch of epicycloidal resonance attractors, as reported earlier [16].

Some of these results were complemented by numerical simulations had used the Oregonator model [19, 20] extended by a term $\phi = \phi(t)$ that accounts for the effect of bromide ions produced by the illumination [21]:

$$\frac{\partial u}{\partial t} = \frac{1}{\epsilon}[u - u^2 - (fv + \phi)\frac{u - q}{u + q}] + D_u\nabla^2 u, \tag{3}$$

$$\frac{\partial v}{\partial t} = u - v. \tag{4}$$

Here, the variables $u$ and $v$ correspond to the concentration of the autocatalytic species $HBrO_2$ and the oxidized form of the catalyst, respectively. Due to the immobilization of the catalyst, variable $v$ does not diffuse in this model. The parameters $\varepsilon = 0.05$, $q = 0.002$ $f = 3.5$ and $D_u = 1$ are kept constant. A series of trajectories of the spiral wave tip simulated under local feedback control is shown in Fig. 5. These simulations are consistent with the epi- and hypocycloidal resonance attractors observed experimentally (see Fig. 2a). A numerical study of the dependence of their radius $R_s$ on $\tau$, as shown in Fig. 6, is in good agreement with the theoretical predictions. There is, however, some discrepancy with the experimental findings (see Fig. 4). In the experiments hypocycloidal resonance attractors are observed in a quite extended range of delay times, whereas the corresponding intervals in theory and simulations are comparatively narrow. This disagreement becomes more pronounced as $\tau$ increases. A possible reason for this is the relaxation and delayed response [22] of the spiral wave in experiments following the application of a light pulse.

## Discussion

Our experimental results show that there are two types of resonance attractors that can be observed for a rigidly rotating spiral wave under local feedback control: an epi- and a hypocycloidal one. Type,

Table 1: Properties of the epi- and hypocycloidal resonance attractor.

| Characteristic Property | Epicycloidal Attractor | Hypocycloidal Attractor |
|---|---|---|
| rotation direction of tip and core | coincide | opposite |
| rotation period, $T_{mp}$ | $> T_u$ | $< T_u$ |
| attractor size | large | small |
| pulse interval location | outer part of the trajectory | inner part of the trajectory |
| effect of increasing | attractor radius decreases | attractor radius increases |

size and stability of the attractor can be changed by introducing a time delay into the feedback loop. In Table 1 some of the characteristic properties are compared with each other.

Tip trajectories corresponding to near-resonance conditions of the two attractors remind one of the resonance drift induced by periodic external forcing of rigidly rotating spiral waves [23]. If $T_{mp}$ and $T_u$ are exactly equal, the perfect resonance is expected, with the core center moving along a straight line. But the period of modulation induced by the local feedback mechanism is just near-resonance, i.e., either $T_{mp} > T_u$ or $T_{mp} < T_u$, therefore the trajectory has either epi- or hypocycloidal shape.

A control parameter that defines the boundary between the two types of attractors is the initial distance $R_0$ between measuring point and core center. In fact, the hypocycloidal shape is observed for $R_0 < 0.15\lambda$, whereas for larger values of $R_0$ only the epicycloidal one appears to be realized. On the other hand, $R_0$ must not be too small, i.e., it must be larger than the core radius, $r_q$. Otherwise, with the measuring point located inside the core no light pulse is triggered. According to ref. [16] the hypocycloidal resonance attractor is reached for the interval $r_q < R_0 < r_0$. In our experiments $r_q = 0.070\lambda$ and $r_0 = 0.152\lambda$ (see insert of Fig. 4). Hence, the boundary value $R_0 < 0.15\lambda$ is in good agreement with theoretical expectations [16].

Interestingly, most of the properties of the hypocycloidal resonance attractor shown in Table 1, which refer to the rigidly rotating spiral waves, are very similar to those of the entrainment attractor for meandering spirals [14, 15], although the dynamics of the rigidly rotating and meandering spirals differ significantly by the fact that their movement is composed of either one (spatially uniform) or two (not spatially uniform) rotation frequencies.

To be noticed is the difference in the modulation period. For rigid rotation it is equivalent to the rotation period at the measuring point $T_{mp}$, where $T_{mp} < T_u$ for the hypocycloidal resonance attractor. On the other hand, for the entrainment attractor of meandering spirals, it is equal or very close to the period $T_0$ at the center of the unperturbed hypocycloidal trajectory. Finally, we point to our observation that the attractor shapes deviate strongly from circular symmetry, if the time delay in the feedback loop becomes relatively long. To study further instabilities of the resonance attractor for such long delays is an interesting challenge for future work.

O.K., S.K. and C.U. thank the Postgraduate Education and Research Program in Chemistry funded by the Royal Thai Government and O.K. thanks the Thailand Research Fund for financial support.

# References

[1] A.T. Winfree, Science 175 (1972) 634.

[2] S.C. Müller, T. Plesser, B. Hess, Science 230 (1985) 661.

[3] O. Steinbock, V.S. Zykov, S.C. Müller, Nature 366 (1993) 322.

[4] V.K. Vanag, L. Yang, M. Dolnik, A.M. Zhabotinsky, I.R. Epstein, Nature 406 (2000) 389.

[5] A.L. Lin, M. Bertram, K. Martinez, H.L. Swinney, Phys. Rev. Lett. 84 (2000) 4240.

[6] T. Sakurai, E. Mihaliuk, F. Chirila, K. Showalter, Science 296 (2002) 2009.

[7] J.M. Davidenko, A.V. Pertsov, R. Solomonsz, W. Baxter, J. Jalife, Nature (London) 355 (1992) 349.

[8] A.V. Panfilov, S.C. Müller, V.S. Zykov, J.P. Keener, Phys. Rev. E 61 (2000) 4644.

[9] F. Xie, Z. Qu, A. Garfinkel, J.N. Weiss, Am. J. Physiol. Heart Circ. Physiol. 280 (2001) 1667.

[10] K.H.W.J. Ten Tusscher, D. Noble, P.J. Noble, A.V. Panfilov, Am. J. Physiol. Heart Circ. Physiol. 286 (2004) 1573.

[11] L. Kuhnert, Naturwissenschaften 73 (1986) 96.

[12] K.I. Agladze, V.A. Davydov, A.S. Mikhailov, JETP Lett. 45 (1987) 767.

[13] M. Braune, H. Engel, Chem. Phys. Lett. 211 (1993) 534.

[14] S. Grill, V.S. Zykov, S.C. Müller, Phys. Rev. Lett. 75 (1995) 3368.

[15] S. Grill, V.S. Zykov, S.C. Müller, J. Phys. Chem. 100 (1996) 19082.

[16] A. Karma, V.S. Zykov, Phys. Rev. Lett. 83 (1999) 2453.

[17] O.-U. Kheowan, V.S. Zykov, O. Rangsiman, S.C. Müller, Phys. Rev. Lett. 86 (2001) 2170.

[18] V.S. Zykov, O.-U. Kheowan, O. Rangsiman, S.C. Müller, Phys. Rev. E 65 (2002) 26206.

[19] R.J. Field, R.M. Noyes, J. Chem. Phys. 60 (1974) 1877.

[20] W. Jahnke, A.T. Winfree, Int. J. Bifur. and Chaos 1 (1991) 445.

[21] H.J. Krug, L. Pohlmann, L. Kuhnert, J. Phys. Chem. 94 (1990) 4862.

[22] M.K. Ram Reddy, M. Dahlem, V.S. Zykov, S.C. Müller, Chem. Phys. Lett. 236 (1995) 111.

[23] V.A. Davydov, V.S. Zykov, A.S. Mikhailov, Sov. Phys. Usp. 34 (1991) 665.

## Output ที่ได้จากโครงการ

**ผลงานที่ตีพิมพ์ในวารสารวิชาการระดับนานาชาติ**

1. Kheowan, O., Kantrasiri S., Uthaisar C., Gáspár V., and Müller, S.C., “Spiral Wave Dynamics Controlled by a Square-Shaped Sensory Domain”*, Chem. Phys. Lett.* **389** (2004) 140. (impact factor: 2.438)
2. Kheowan, O., Kantrasiri S., Wilairat P., Storb U., and Müller, S.C., “Spiral wave dynamics under feedback control derived from a variety of sensory domains”*, Phys. Rev.* E **70** (2004) 46221-46225. (impact factor: 2.202)
3. Kheowan, O., Uthaisar C., Kantrasiri S., and Müller, S.C., “Hypocycloidal resonance attractor for rigidly rotating spiral waves”*, Chem. Phys. Lett.* **399** (2004) 506-511. (impact factor: 2.438)

# ภาคผนวก

Available online at www.sciencedirect.com
SCIENCE DIRECT®
Chemical Physics Letters 389 (2004) 140–144
CHEMICAL PHYSICS LETTERS
www.elsevier.com/locate/cplett

# Spiral wave dynamics controlled by a square-shaped sensory domain

On-Uma Kheowan [a,*], Supichai Kantrasiri [a], Chananate Uthaisar [a], Vilmos Gáspár [b], Stefan C. Müller [c]

[a] Department of Chemistry, Mahidol University, Rama 6 Road, Bangkok 10400, Thailand
[b] Institute of Physical Chemistry, University of Debrecen, P.O. Box 7, H-4010 Debrecen, Hungary
[c] Institut für Experimentelle Physik, Otto-von-Guericke-Universität, Universitätsplatz 2, D-39106 Magdeburg, Germany

Received 6 February 2004; in final form 17 March 2004

**Abstract**

Spiral waves rotating rigidly in a thin layer of the light-sensitive Belousov–Zhabotinsky (BZ) reaction are subjected to a time-dependent uniform illumination. A non-local feedback algorithm computes the illumination intensity to be proportional to the average wave activity within a square-shaped sensory domain. The investigations show a broad spectrum of dynamical responses which results in square- and cross-shaped trajectories of the spiral tip, including reflections at the virtual walls. The geometry of the sensory domain is crucial in determining size and shape of the tip trajectories. A theoretical approach is proposed to explain the observed phenomena.


Controlling the evolution of complex processes in time and space is a major research issue of nonlinear dynamics [1,2]. It is important for many dynamical phenomena including the formation of spatio-temporal patterns in chemical reactions like the CO oxidation on platinum surfaces [3,4] or the Belousov–Zhabotinsky (BZ) reaction [5,6]. Some of the effective control methods have been applied to chemical waves propagating in excitable media, such as external (periodic) forcing [7–9]. Methods involving a time-delayed feedback [2], require more complex algorithms [10,11] that are based on collecting data on the activity level of the medium.

In this report we investigate spiral waves rotating in an excitable layer of the BZ reaction. The activity level in this medium can be measured at one point (local feedback) [9,12], in a given domain (non-local feedback) [13,14] and at all points (global feedback) [10]. Of both theoretical and practical interest is the effect of shape and size of the applied 'sensory domain' on the dynamics of rotating spiral waves under feedback control. We apply square-shaped domains and find a broad spectrum of dynamical responses, including square-shaped and cross-shaped trajectories of the spiral tip. Numerical simulations using the light-sensitive Oregonator model [15,16] reproduce this behaviour. We suggest that the feedback method introduced in this work offers an efficient tool for controlling also the dynamics of other excitable media.

We study spiral wave dynamics in thin layers of the BZ reaction with the light-sensitive $Ru(bpy)_3^{2+}$ catalyst [17]. This catalyst promotes the autocatalytic production of $HBrO_2$, the activator species of the BZ system. The applied illumination enhances the production of the bromide ion, an inhibitor species, and thus decreases the system's excitability which, in turn, results in slowing down the wave activity in the medium. This provides an experimentally accessible method to control spiral wave dynamics, in that the light intensity influences parameters such as the wavelength and the diameter of the spiral core.

In our experiments, the $Ru(bpy)_3^{2+}$ catalyst was immobilized in a silica gel matrix [18] (thickness 0.3 mm, diameter 5 cm) at a concentration of 4.2 mM. The reactants and their concentrations (disregarding bromination of malonic acid) were: $NaBrO_3$ (0.20 M), malonic acid (0.17 M), $H_2SO_4$ (0.39 M) and NaBr (0.09 M) [12]. The experiments were carried out at an ambient

* Corresponding author. Fax: +662-2458332.
*E-mail address:* scokw@mucc.mahidol.ac.th (O.-U. Kheowan).

0009-2614/$ - see front matter © 2004 Elsevier B.V. All rights reserved.
doi:10.1016/j.cplett.2004.03.077

temperature of $25 \pm 1$ °C. We created a spiral wave by using a spot (diameter, 1 cm) of intense light from a cold light source to break a propagating wave front (this creates two wave ends) and suppressing one of the open ends with the light spot to leave a single spiral in the center of the dish [12]. The reaction layer was uniformly illuminated from below with a video projector controlled by a computer via a frame grabber. The oxidation waves were observed in transmitted light by a CCD camera and stored on a computer. The main features of spiral rotation, the trajectory of spiral tip, is determined by a special computer procedure given in [9].

In our non-local feedback algorithm, the illumination intensity applied to the reaction layer is given by Kheowan et al. [13]

$$I(t) = I_0 + k_{\mathrm{fb}}[B(t) - B_0], \tag{1}$$

where $I_0$ is a constant background intensity. $B(t)$ is the average grey level of the pixels in the square-shaped sensory domain

$$B(t) = \frac{1}{n}\sum_{i=1}^{n} G_i(t), \tag{2}$$

where $0 \leqslant G_i \leqslant 255$ is the grey level of a given pixel, and $n$ is the total number of pixels in the domain. Note that a larger grey level corresponds to higher concentration of the oxidized form of the catalyst (bright fronts). The intensity of the feedback illumination $I(t)$ is controlled by the gain $k_{\mathrm{fb}}$, and the value of $B(t)$. The constant $B_0$ is the $B(t)$ averaged over one period of a spiral placed in the center of the square domain and illuminated with background intensity $I_0$.

The effects of such non-local feedback on a rigidly rotating spiral wave are shown in Fig. 1. For a side length $d$ of the domain significantly smaller than the spiral wavelength $\lambda$ ($d = 0.5\lambda$), the spiral leaves the center of the sensory domain, where its circular core was initially placed (arrow in Fig. 1a), by drifting outwards until it makes a turn to follow a circular path with a radius of about $0.76\lambda$. This motion resembles that observed in earlier reported experiments applying a small size, circular-shaped sensory domain [13].

For a domain size equal to the spiral wavelength ($d = \lambda$), the spiral core first drifts away from the domain center (Fig. 1b), then it approaches a stable, square-shaped trajectory with a side length of about $1.33\lambda$, which is rotated by about 45° with respect to the domain. Note that the drift velocity of the spiral wave core changes periodically: it is slower at the corners and faster at the sides of the trajectory.

Fig. 1c shows the trajectory of the spiral tip in an experiment with a still larger feedback domain, $d = 1.25\lambda$. In this case, the spiral tip was initially placed close to the domain boundary. The feedback control induces first a drift towards the center and subsequently towards the middle region of the adjacent side of the domain. This process occurs several times and consequently the spiral tip is caught inside the square, bouncing from and to the 'virtual walls'. Fig. 1a–c indicate that increasing the size $d$ of the feedback domain has a pronounced effect on the shape and size of the spiral tip trajectory. In certain ranges of increasing $d$, the size of the square trajectory is reduced. Experiments also show that the trajectories act like attractors: the spiral tip always approaches them independently from its initial position.

We complemented the experiments by numerical simulations using the Oregonator model [15], extended by a term $\phi = \phi(t)$ accounting for the effect of bromide ion produced due to the illumination [16]:

$$\frac{\partial u}{\partial t} = \frac{1}{\epsilon}\left[u - u^2 - (fv + \phi)\frac{u - q}{u + q}\right] + \nabla^2 u, \tag{3}$$

$$\frac{\partial v}{\partial t} = u - v. \tag{4}$$

Here, the variables $u$ and $v$ describe the evolution of the concentration of the autocatalytic species $HBrO_2$ and

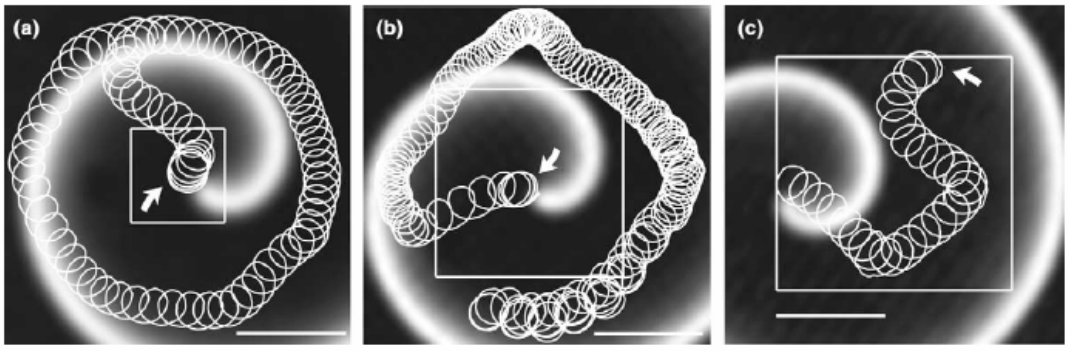


Fig. 1. Experimental trajectories of a spiral wave tip subjected to the feedback control Eqs. (1) and (2) for different sizes of the sensory domain: (a) $d = 0.5\lambda$ ($\lambda$ = spiral wavelength) with $B_0 = 24$, $k_{\mathrm{fb}} = 0.2$, (b) $d = 1.0\lambda$ with $B_0 = 24.5$, $k_{\mathrm{fb}} = 0.8$, and (c) $d = 1.25\lambda$ with $B_0 = 19$, $k_{\mathrm{fb}} = 0.45$. $I_0 = 0.70$ mW cm$^2$ for all experiments. The domains and the initial spiral core locations are indicated by squares and thick arrows, respectively. The spiral images are shown for the start of the trajectory in (a) and (b) and the end of the trajectory in (c). Scale bar: 1 mm.

the oxidized form of the catalyst, respectively. Due to the immobilization of the catalyst, variable $v$ does not diffuse in this model. The parameters $\varepsilon = 0.05$, $q = 0.002$ and $f = 3.5$ are kept constant. Non-local feedback is introduced into the model by varying the value of $\phi(t)$ according to [10]

$$\phi(t) = \phi_0 + k_{\mathrm{fb}}[\tilde{B}(t) - \tilde{B}_0], \tag{5}$$

$$\tilde{B}(t) = \frac{1}{S}\int_s v\mathrm{d}s, \tag{6}$$

where $\phi_0$ is constant ($=0.01$). The integral $\tilde{B}(t)$ takes into account the effect of the average wave activity in the square-shaped sensory domain $S$. The constant $\tilde{B}_0$ refers to this integral averaged over one period of a spiral placed in the domain center with constant production term $\phi(t) = \phi_0$.

Fig. 2a shows the result of calculations based on Eqs. (3)–(6) with $d = \lambda$ (41 s.u.) and $k_{\mathrm{fb}} = 0.1$. The spiral core was initially located at the center of the sensory domain. Switching on the feedback control induces the drift of the spiral core first outwards from the center and then along a square-shaped trajectory, in good agreement with the experimental results (Fig. 1b). In the parts of the trajectory labeled 1 and 4 the center of the core drifts approximately along a straight line. In part 2 the trajectory starts to bend and to slow down and then turns by 90° in part 3. Corresponding changes in the illumination intensity $\phi(t)$ are shown in Fig. 2b. The feedback algorithm is turned on at $t = 20$ (after about 3 rotations) resulting in large amplitude oscillations of the $\phi$ values. To show a slight shift in the phase of this oscillation, black dots have been plotted on the abscissa at an interval equal to the oscillation period measured at the part of the trajectory labeled 1. Using these 'stroboscopic' dots, the phase shift, for example, between points labeled 1 and 4 can be determined as $0.54\pi$, which agrees well with the angle difference of the drift directions (90°) at points 1 and 4 of the square-shaped trajectory in Fig. 2a.

The oscillations in $\phi(t)$ are due to corresponding changes of the value of the integral in Eq. (6), which we analyze by considering unperturbed spirals (without feedback) placed inside and outside the quadratic sensory domain. The location of the spiral tip is indicated by black circles labeled with letters P–S, as indicated in the quadratic insert of Fig. 2c. These black circles depict

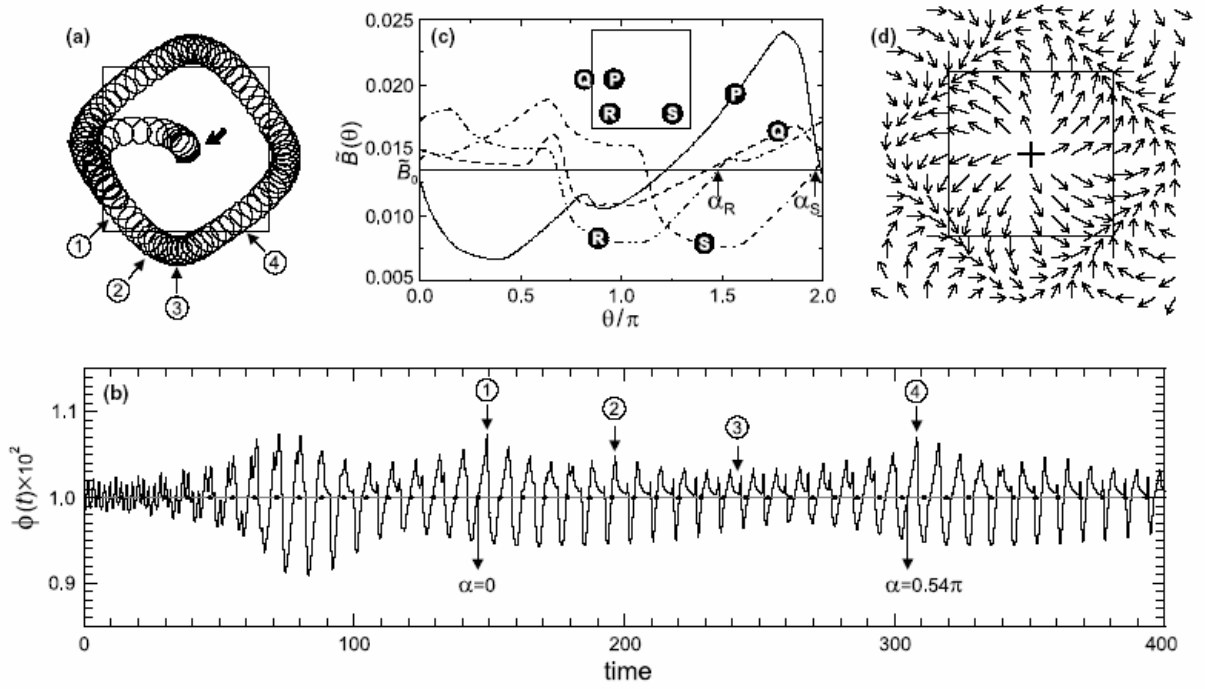


Fig. 2. Spiral wave simulated by Eqs. (3)–(6) under feedback control derived from a square domain with $d = \lambda$. The computations were performed by the explicit Euler method, using a five-point approximation of the Laplacian on a $384\times384$ array with a grid spacing $\Delta x = 0.5$ and time step triangle $t = 0.001$. (a) Trajectory of spiral wave tip under a feedback control with $k_{\mathrm{fb}} = 0.10$. (b) Value of $\phi(t)$ corresponding to the trajectory in (a). The feedback was switched on at time = 20. $\alpha$ is the rotation phase. (c) Analysis of integral (Eq. (6)) as a function of the rotation angle $\theta$ of the spiral wave (without feedback) for different locations of the spiral wave core. Each curve is labeled by letters that correspond to those in the square domain (inset) and indicate the location of the spiral core. $\tilde{B}_0$ is the average value of $\tilde{B}(\theta)$ for one rotation of a spiral placed at the domain center. Rotation phases given by arrows are: $\alpha_R = 1.48$, $\alpha_S = 1.97$. (d) Flow map of spiral core trajectory. Arrows indicate the velocity and the direction of the drift. Distance between data points is $1/8\lambda$. The direction of each vector is determined from the difference between the phase of $\tilde{B}$ at that point (arrow tail) and a reference phase (in this case $\pi/4$). Its modulus is calculated as the integral of $|\tilde{B}(\theta)-\tilde{B}_0|$ over one period of the rotation angle $\theta$.

the locations of the spiral core along the trajectory in Fig. 2a. For example, points R and S in the insert correspond to the parts of the trajectory in Fig. 2a, labeled 1 and 4, respectively.

The $\tilde{B}$-values are calculated and plotted in Fig. 2c for one rotation of the spiral ($0 \leqslant$ rotation angle $\theta \leqslant 2\pi$), without feedback. Here, $\tilde{B}$ can be written as a function of the rotation angle $\theta(t)$, which is proportional to time $t$, i.e. $\tilde{B} = \tilde{B}(\theta)$. The horizontal line in this graph corresponds to $\tilde{B}_0$, as specified in the caption. Curves $\tilde{B}(\theta)$ oscillate with different shape and amplitude for different locations P–S. Considering the extrema of these curves $\tilde{B}(\theta)$, their high values at location P result in a large perturbation and therefore, a fast drift of the spiral wave core, as observed in Fig. 2a. Around location Q, corresponding to one of the corners of the square-shaped trajectory in Fig. 2a, the values of these extrema drop, therefore, the drift around the corners is slow. In order to explain the direction of the drift, the phase of curve $\tilde{B}(\theta)$ must be characterized. Note that all shown curves cross the reference line, $\tilde{B}(\theta) = \tilde{B}_0$, with a positive slope only once during a rotation period. In order to further characterize these curves, the value of the rotation angle at the intersections is defined as the rotation phase $\alpha$. One can see that the shapes of the $\tilde{B}(\theta)$ curves at locations R and S (with drift directions that are perpendicular to each other) are similar, but their phases differ by about $0.5\pi$ (compare $\alpha_R$ and $\alpha_S$ in Fig. 2c). This corresponds well to the phase shift of $0.54\pi$ in the feedback signal in parts 1 and 4 of Fig. 2b.

For a more detailed analysis, the local values of $\tilde{B}(\theta) = \tilde{B}_{x,y}(\theta)$ were determined on a finer grid of core locations $(x, y)$. This provides the possibility to construct a flow map shown in Fig. 2d. As described in the caption, this flow map is based on phases representing the drift directions. The integral of $|\tilde{B}(\theta)-\tilde{B}_0|$ over one period is taken as a measure for the magnitude of the perturbation and represents the drift velocity. Most of the flow vectors are attracted towards a square trajectory, on which they are caught in a counterclockwise motion, in agreement with the observed attractor in Fig. 2a.

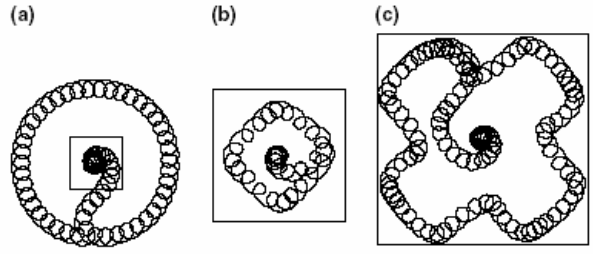


Fig. 3. Simulation results of the spiral wave dynamics under a feedback control derived from different sizes of the domain: (a) $d = 0.5\lambda$, $k_{fb} = 0.10$, (b) $d = 1.25\lambda$, $k_{fb} = 0.20$, and (c) $d = 2\lambda$, $k_{fb} = 0.50$. Trajectories (a) and (b) correspond to experiments shown in Fig. 1a and c, respectively.

The dynamics of such an attractor changes with the size of the integration domain. For a rather small domain ($d = 0.5\lambda$) one obtains a circular attractor (Fig. 3a), similar to that of Fig. 1a. Here, the four-fold geometry of the sensory domain is not reflected in the shape of the trajectory. For domains larger than the spiral wavelength, the size of the attractor decreases, as shown in Fig. 3b where $d = 1.25\lambda$. The 90° turns of the drift direction close to the virtual walls agree with the experimental observation (Fig. 1b). An interesting cross-shaped trajectory is created by further increasing the domain (Fig. 3c).

Our experimental and numerical results demonstrate that the considered nonlocal feedback algorithm is highly efficient to control spiral wave dynamics. The method can be transferred to control such dynamics in other types of spatially extended systems, e.g. in cardiac [19] and neuronal tissue [20] or in the context of intracellular calcium dynamics [21]. The size and shape of a sensor by which we collect information about the activity level of a dynamical system turns out to be crucial and decisive on determining the size and shape of the spatio-temporal attractor governing the behaviour of the system under feedback control.

## Acknowledgements

The authors acknowledge the contribution of R. Csillag to the preliminary experiments and thank U. Storb for useful discussions. O.K., S.K. and C.U. thank the Postgraduate Education and Research Program in Chemistry funded by the Royal Thai Government for financial support. O.K. thanks the Thailand Research Fund and V.G. thanks OTKA T038071 for financial support.

## References

[1] H.G. Schuster (Ed.), Handbook of Chaos Control, Wiley-VCH, Weinheim, 1999.
[2] K. Pyragas, Phys. Rev. E 66 (2002) 26207.
[3] S. Jakubith, H.H. Rotermund, W. Engel, A. von Oertzen, G. Ertl, Phys. Rev. Lett. 65 (1990) 3013.
[4] M. Kim, M. Bertram, M. Pollmann, A. von Oertzen, A.S. Mikhailov, H.H. Rotermund, G. Ertl, Science 292 (2001) 1357.
[5] A.T. Winfree, Science 175 (1972) 634.
[6] A.L. Lin, M. Bertram, K. Martinez, H.L. Swinney, A. Ardelea, G.F. Carey, Phys. Rev. Lett. 84 (2000) 4240.
[7] K.I. Agladze, V.A. Davydov, A.S. Mikhailov, JETP Lett. 45 (1987) 767.
[8] O. Steinbock, V.S. Zykov, S.C. Müller, Nature 366 (1993) 322.
[9] S. Grill, V.S. Zykov, S.C. Müller, Phys. Rev. Lett. 75 (1995) 3368.
[10] V.S. Zykov, A.S. Mikhailov, S.C. Müller, Phys. Rev. Lett. 78 (1997) 3398.
[11] T. Sakurai, E. Mihaliuk, F. Chirila, K. Showalter, Science 296 (2002) 2009.

[12] O. Kheowan, V.S. Zykov, O. Rangsiman, S.C. Müller, Phys. Rev. Lett. 86 (2001) 2170.
[13] O. Kheowan, C.K. Chan, V.S. Zykov, O. Rangsiman, S.C. Müller, Phys. Rev. E 64 (2001) 35201.
[14] V.S. Zykov, G. Bordiougov, H. Brandtstädter, I. Gerdes, H. Engel, Phys. Rev. Lett. 92 (2004) 18304.
[15] W. Jahnke, A.T. Winfree, J. Bifur. Chaos 1 (1991) 445.
[16] H.J. Krug, L. Pohlmann, L. Kuhnert, J. Phys. Chem. 94 (1990) 4862.
[17] V. Gáspár, Gy. Bazsa, M.T. Beck, Z. Phys. Chem. (Leipzig) 264 (1983) 43.
[18] T. Yamaguchi, L. Kuhnert, Zs. Nagy-Ungvarai, S.C. Müller, B. Hess, J. Phys. Chem. 95 (1991) 5831.
[19] J.M. Davidenko, A.V. Pertsov, R. Salomonsz, W. Baxter, J. Jalife, Nature (London) 355 (1992) 349.
[20] M. Dahlem, S.C. Müller, Exp. Brain Res. 115 (1997) 319.
[21] M. Falcke, Y. Li, J.D. Lechleiter, P. Camacho, Biophys. J. 85 (2003) 1474.

# Spiral wave dynamics under feedback control derived from a variety of sensory domains

On-Uma Kheowan,* Supichai Kantrasiri, and Prapin Wilairat
*Department of Chemistry, Mahidol University, Rama 6 Road, Bangkok 10400, Thailand*

Ulrich Storb and Stefan C. Müller
*Institut für Experimentelle Physik, Otto-von-Guericke-Universität Magdeburg, Universitätsplatz 2, D-39106 Magdeburg, Germany*
(Received 11 May 2004; published 29 October 2004)

The dynamics of rigidly rotating spiral waves in a reaction layer with light-dependent excitability is studied by numerical integration of a reaction-diffusion equation system with a feedback control. The feedback signal is derived from sensory domains with different geometries by introducing an algorithm that computes the illumination intensity to be proportional to the average wave activity in these domains. It is shown that the shape and size of the trajectories of the spiral wave tip as well as the stability of the spiral rotation depend sensitively on the choice of the geometry of the sensory domain. The numerically observed effects are complemented by constructing a flow map based on an analysis of the feedback signal.

DOI: 10.1103/PhysRevE.70.046221 PACS number(s): 05.45.−a, 05.65.+b, 47.54.+r

## I. INTRODUCTION

The implementation of control strategies to manipulate complex oscillations and spatiotemporal patterns has become a central issue of nonlinear dynamics. Feedback methods provide one of the possible control techniques that yield new modes of spatiotemporal behavior [1,2]. These techniques may be designed in different ways. A feedback is global or nonlocal, in contrast to local techniques, if the control signal represents a sum of contributions from all or many parts of the system. Such feedbacks have been used, for instance, to control spatiotemporal activity in the Pt-catalyzed oxidation of CO [3], suggesting a means for enhancing catalytic efficiency [4], in gas discharges to suppress plasma instabilities [5], in electrochemical systems to influence spatial coupling among different active sites [6], and in semiconductors in connection with charge transport phenomena [7]. Propagating waves [8] and, in particular, spiral waves [9–12] in the Belousov-Zhabotinsky (BZ) reaction [13,14] have also been controlled by using these feedback methods, which points to the possibility of manipulating dynamical patterns in excitable media including excitable biological tissues [15–17]. A recent advance in this direction is the control of seizurelike events in hippocampal brain slices with adaptive electric fields [18]. Thus, the ability to regulate spatiotemporal behavior provides both a means of generating desired dynamical patterns and the tools for probing underlying mechanisms.

In this work we perform a numerical study of rigidly rotating spiral waves subjected to a nonlocal feedback derived from a confined "sensory domain." A time-dependent spatially uniform modulation of the system's excitability is taken to be proportional to the integral light absorption observed within this domain. Of both theoretical and practical interest are the geometrical features of the applied sensory domain on the dynamics of the rotating spirals [9–13]. We apply the feedback with different shapes and sizes of the domain and find a broad spectrum of dynamical responses, including various shapes of the spiral tip trajectories and the switching between their stability properties. A flow map and a bifurcation diagram are constructed in order to analyze the observed phenomena.

## II. SIMULATION METHOD

Our computations are performed with the light-sensitive two-variable Oregonator model [19–21], which has been successfully used to describe the dynamics of the photosensitive BZ system by including a flux term $\phi=\phi(t)$ for the light-induced bromide production [21]:

$$\frac{\partial u}{\partial t} = D_u \nabla^2 u + \frac{1}{\epsilon}\left[ u - u^2 - (fv + \phi)\frac{(u-q)}{(u+q)} \right], \tag{1}$$

$$\frac{\partial v}{\partial t} = u - v. \tag{2}$$

Here, the variables $u$ and $v$ describe the evolution of the concentration of the autocatalytic species $HBrO_2$ and the oxidized form of the catalyst, respectively. $D_u=1$ is the scaled diffusion coefficient of variable $u$. The catalyst is assumed to be immobilized in a gel matrix; thus, the variable $v$ does not diffuse in this model ($D_v=0$). The parameters have the values $\varepsilon=0.05$, $q=0.002$, and $f=3.5$, which are kept constant. The computations were performed by an explicit Euler method, using the five-point approximation of the Laplacian on a $384\times384$ array with a grid spacing $\Delta h=0.5$ s.u. and time step $\Delta t=0.001$ t.u..

The feedback signal is determined by the integral of wave activity taken over the sensory domains, expressed as [22]

$$\phi(t) = \phi_0 + k_{fb}[\tilde{B}(t) - \tilde{B}_0], \tag{3}$$

with

*Author to whom correspondence should be addressed. Electronic mail: scokw@mucc.mahidol.ac.th

 

$$\tilde{B} = \int_S u dS, \tag{4}$$

where $\phi_0$ is constant (=0.01). Thus, the intensity of the feedback signal is controlled by the coefficient $k_{fb}$ and depends linearly on the integral value $\tilde{B}$ of the variable $u$ over the domain $S$. The constant $\tilde{B}_0$ refers to this integral averaged over one period of a spiral placed in the domain center with constant flux term $\phi(t)=\phi_0$.

## III. RESULTS

A single spiral is induced from the equation system (1) and (2) by choosing a special initial condition [23]. The variables $u$ and $v$ are initially set to zero uniformly in the medium. To create a spiral then we introduce a nonuniform distribution of the variables. A superthreshold value $u=1$ is given along a line near the boundary of the excitable medium to induce a propagating wave. After this wave has reached the center of the excitable medium, one-half of the planar wave is erased by resetting $u=v=0$. Subsequently, the open end of the planar wave curls into a spiral wave with its core located near the center of the excitable medium. Without external forcing and with the above chosen parameter values, the spiral wave rotates rigidly around a circular core with a rotation period $T_0=8.2$ t.u. and a wavelength $\lambda=4.1$ s.u.. There is ample evidence [9–11,22] that for this kind of nonlocal feedback a spiral wave core placed initially at the center of the sensory domain is destabilized for the case of a positive coupling constant $k_{fb}$ and starts to drift away from the center, as shown in all of the examples of Fig. 1. A previous systematic study of circular sensory domains has shown that it frequently moves asymptotically on a circular attractor [9].

In our simulations we find how the shape of this type of spiral tip trajectories is transformed when the shape of the sensory domain is varied. For a triangular domain the feedback induces the spiral core to drift away from the domain center and to make a turn on each side with an overall 120° change of the drift direction. Finally it describes a trajectory with an approximately threefold symmetry [Fig. 1(a)]. An increase of the number of corners of the sensory domain results in an increase of the number of turning points of the drift direction, as shown in Figs. 1(b) and 1(c). For a square-shaped domain [Fig. 1(b)], the trajectory describes a square-shaped pathway, which is rotated by about 45° with respect to the domain. A further increase in the number of domain corners to form a pentagon [Fig. 1(c)] produces a trajectory that follows an approximately pentagonal pathway inside the domain. It appears to be almost circular, because the five rounded corners of the domain are only faintly reflected. For perfect symmetry, as for the circular domain in Fig. 1(d), the trajectory describes a circular pathway around the domain.

Exerting some shear on the square-shaped domain causes a transformation of the trajectory from a square to a rhombic pathway, as shown in Figs. 1(e) and 1(f). A further decrease of the acute angle of the rhombus induces the trajectory to form a large oblong excursion around the domain [Fig. 1(g)].

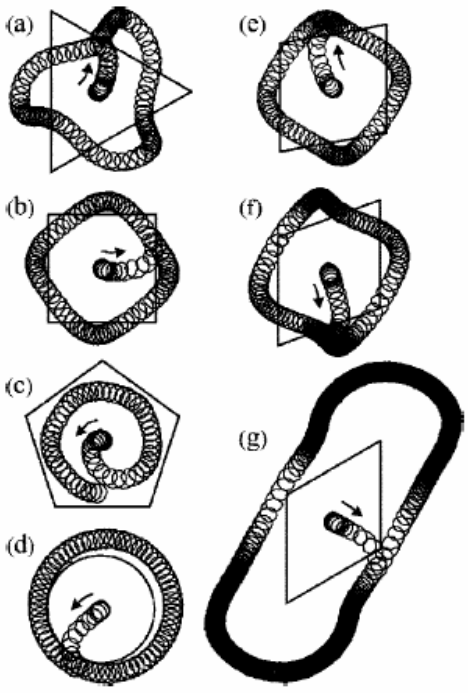


FIG. 1. Trajectories of the spiral wave tip derived from simulations for different shapes of the sensory domain starting from an initial location of the spiral core at the domain center. (a) Triangle, side length 1.50λ, $k_{fb}=0.05$; (b) square, side length 1.00λ, $k_{fb}=0.11$; (c) pentagon, side length 0.75λ, $k_{fb}=0.15$; (d) circle, diameter 1.00λ, $k_{fb}=0.08$; (e)–(g) rhombus, side length 1.00λ and $k_{fb}=0.10$; acute angles: 80°, 70°, and 60°, respectively. The feedback mechanism is computed from Eqs. (3) and (4). Arrows indicate drift direction of the spiral core.

Now the drift velocity of the spiral wave core changes drastically along the oblong pathway. It becomes very slow when the spiral wave core is far away from the center of the rhombic domain. The results demonstrate that the shape of the sensory domain is reflected in the dynamics of the spiral tip trajectory.

Besides the shape of the domain it is also its size that plays a crucial role for the spiral dynamics, as shown in Fig. 2. We use the square-shaped domain with side length $d_s$ to study this effect. For a rather small size ($d_s=0.7\lambda$) one obtains a circular attractor [Fig. 2(a)], not reflecting the fourfold symmetry of the sensory domain. The circular trajectory transforms to a square for $d_s=1.0\lambda$ [Fig. 2(b)], similar to the one in Fig. 1(b). For domains larger than the spiral wavelength the size of the attractor decreases, as shown in Fig. 2(c) where $d=1.25\lambda$.

Note that the drift velocity in Fig. 2(b) is larger than that in Fig. 1(b). This increase is connected with the choice of a larger feedback coupling strength. In fact, we found that for fixed size and shape of the sensory domain larger $k_{fb}$ values lead to a faster drift, as long as the shape of the tip trajectory is rather simple as, for instance, for the case of square domains with size $d_s<1.5\lambda$. For larger $d_s$ the tip dynamics becomes complex (see below) and the influence of $k_{fb}$ cannot be easily predicted.

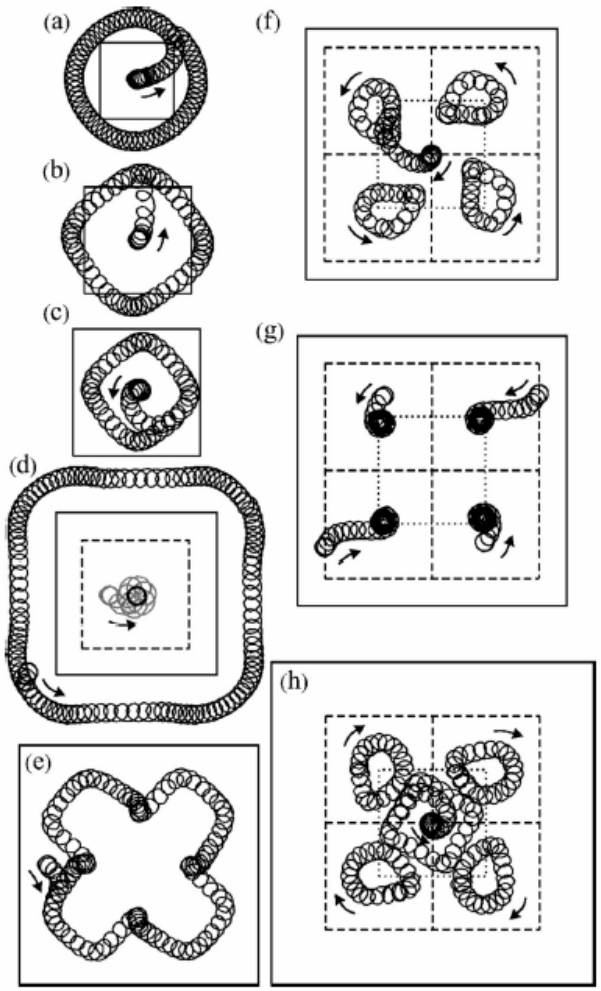


FIG. 2. Trajectories of spiral wave tip under variation of the size of the square domain. (a)–(h) Side length $d_s$=0.70λ, 1.00λ, 1.25λ, 1.50λ, 2.25λ, 2.40λ, 2.50λ, 3.00λ; $k_{fb}$=0.05, 0.15, 0.12, 0.20, 0.40, 0.50, 0.50, 0.75. Arrows indicate the drift direction of the spiral core. The dashed squares with $d_s$=λ indicate the approximate location of the separatrix of basins of attraction, whereas the dotted squares depict a reference domain ($d_s$=λ). The gray curve in (d) shows the transient trajectory, before a circular, stable rotation is achieved at the center (black circle).

Two trajectories are observed for $d_s$=1.50λ [Fig. 2(d)]. A small, flowerlike trajectory occurs at the center of the domain, when the unperturbed spiral core is initially placed close to the domain center. Note that the gray curve in Fig. 2(d) represents the transient trajectory before a circular, stable rotation (black circle) is achieved at the center. For a larger initial distance to the domain center, the spiral core is attracted towards a trajectory describing a large square with rounded corners. Its orientation coincides with that of the domain, in contrast to the trajectories in Figs. 2(b) and 2(c), which are rotated by about 45° with respect to the domain. The dashed square with side length λ in Fig. 2(d) indicates the approximate location of the separatrix between two basins of attraction that exist for the motion of the spiral core center. However, the attractor, which is eventually reached, is determined not only by the initial location of the spiral core but also by the initial location of the tip with respect to the core center (the initial phase). Thus the location of the separatrix depends on this initial phase, which slightly blurs this separating line. We checked numerically that the blurring effect of the initial phase is below 0.024λ.

An interesting cross-shaped trajectory is created when increasing the domain size to $d_s$=2.25λ [Fig. 2(e)]. This trajectory can be considered as a combination of four small pieces of square-shaped trajectories, which are linked together. With a further increase of $d_s$ to 2.40λ, there appear four trajectories, which are separated from each other [Fig. 2(f)]. Note that the shape of the trajectories changes from a squarelike to a droplike form. Which of these four possible stable orbits is reached depends now on the initial location of the unperturbed spiral core center. The approximate separatrices between the basins of attraction of each orbit are shown by dashed boxes [Fig. 2(f)].

The dynamics of the four attractors in Fig. 2(f) can be stabilized by enlarging the domain to $d_s$=2.50λ [Fig. 2(g)]; the unperturbed spiral wave core is placed at four different locations inside the domain. The feedback induces the spiral wave core to drift towards four stable points (indicated by arrows), located approximately at the corners of the reference domain $d_s$=λ [dotted square in Fig. 2(g)]. At these points, the spiral rotates rigidly without drift. When the domain size is further increased to $d_s$=3.00λ, the locations of these four points become again unstable [Fig. 2(h)]; i.e., the spiral wave drifts again along a droplike pathway. Note that the drift direction of these droplike attractors is clockwise and the petals of the loopy trajectories are directed outwards, in contrast to those in Fig. 2(f). In addition, a new square-shaped trajectory with inward directed petals appears around the center of the domain.

The dynamics of the trajectories in Fig. 2 can be divided into two types: stable and unstable spiral rotation. Stable rotation means that the spiral rotates rigidly without drift, as illustrated by the trajectories in Figs. 2(d) (small attractor at the center) and 2(g). All other trajectories in Fig. 2 for which the motion of spiral waves is accompanied by a drift of the spiral wave core are considered as an unstable rotation. These results demonstrate that enlarging the domain size leads to a series of switches from unstable to stable spiral rotation and vice versa.

## IV. DISCUSSION

Our discussion is based on the analysis of the integral $\widetilde{B}$ [Eq. (4)] as a function of the rotation angle of spirals placed at different locations inside or outside the square-shaped control domain. It has been shown that the phase of the signal $\widetilde{B}$, which determines the phase of the modulation [Eq. (3)], predominantly affects the drift direction and consequently the shape of the trajectory [12]. The average area under this curve is an appropriate measure for the drift velocity in the range of the sensory domains considered here [12]. The phase relation and the average area form the basis of the flow maps constructed inside and outside the sensory domains as

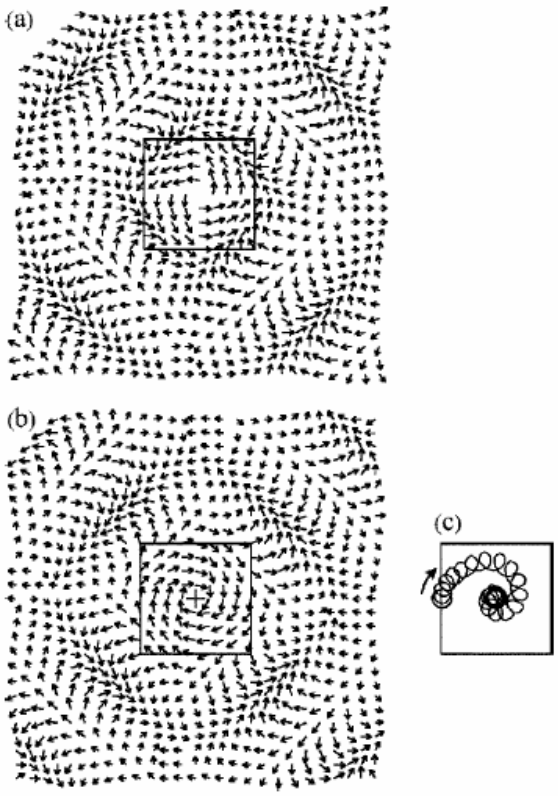


FIG. 3. (a), (b) Vector field plots of the trajectories of the spiral core center under feedback control derived from a square domain with $d_s=\lambda$ for positive feedback (a) and negative feedback (b). (c) Trajectory of the spiral wave tip under negative feedback control with feedback parameters $d_s=1\lambda$ and $k_{fb}=-0.15$. The arrow indicates the drift direction of the spiral core. Note that the coefficient $k_{fb}$ is not involved in the construction of the vectors in the flow map.

shown, for instance, in Fig. 3 for $d_s=\lambda$. The flow vectors observed for positive feedback [Fig. 3(a)], which corresponds to the simulation results observed for $k_{fb}>0$ in Figs. 1(b) and 2(b), are attracted towards two square-shaped trajectories (side length about $1\lambda$ and $3\lambda$) on which they are caught in a counterclockwise motion. The flow map unravels the existence of a discrete set of stable square-shaped orbits, which appear to be attractors for the spiral core drift. The innermost trajectory corresponds to the attractor presented in Figs. 1(b) and 2(b). For the flow map observed for negative feedback [Fig. 3(b)], which is obtained by considering the signal $\tilde{B}$ mirrored with respect to the reference line $B=B_0$ corresponding to negative sign of $k_{fb}$ in Eq. (3), most of the flow vectors inside the domain spiral slowly into the domain center to form a stabilized rotation. This stabilization is confirmed by the simulation result for the tip motion in Fig. 3(c). In a certain region outside the domain the vectors flow towards a square-shaped trajectory with a side length of about $2\lambda$. These flow maps illustrate how the dynamics of the spiral wave can be drastically changed by switching the sign of the feedback gain.

Additional flow maps of the spiral core center under variation of the domain size are shown in Fig. 4. The flow map for the domain with $d_s=1.50\lambda$ is depicted in Fig. 4(a). Here, most of the vectors are attracted towards two types of stable states: a fixed point at the center and a square-shaped orbit in agreement with the trajectories in Fig. 2(d). The basin of attraction of the two states are separated by the separatrix indicated by the dashed square with side length $\lambda$. Solid, open, and checked circles in this figure indicate three types of fixed points: (i) the stable node (solid circle), which attracts the vector field from all directions, (ii) the unstable node (open circle), which repels the vector field in all directions, and (iii) the saddle point, which attracts the vector in one direction but repels it in the direction perpendicular to it. For the flow map in Fig. 4(a) there is one stable node located at the center of the domain. It corresponds to the stabilization of rigid rotation and thus to the small attractor in Fig. 2(d). In addition to the stable node at the center of Fig. 4(a), there appear four unstable nodes at the corners and four saddle points on the edges of the reference domain (dashed square).

The flow map for a larger domain ($d_s=2.50\lambda$) is shown in Fig. 4(b). It corresponds to the trajectories in Fig. 2(g). The locations of the four stable nodes in this map coincide with those of the unstable ones for $d_s=1.5\lambda$ [Fig. 4(a)]. Since the distribution of neighboring nodes for each of them is equal to

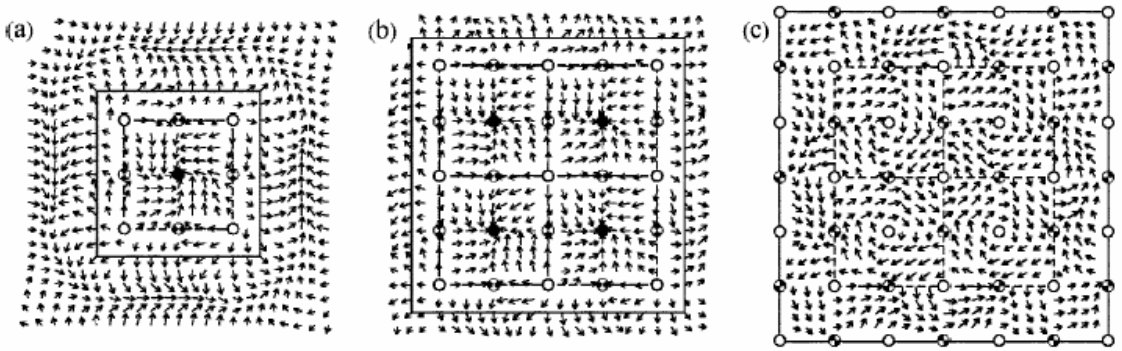


FIG. 4. Flow maps of the spiral core center under variation of the domain sizes for positive feedback, for (a) $d_s=1.50\lambda$, (b) $d_s=2.50\lambda$, and (c) $d_s=3.00\lambda$. Vectors show the drift direction of the spiral core center, which its size indicates the drift velocity. The dashed line indicates the location of the separatrix, which restricts the basin of each attractor. Solid, open, and checked circles indicate the fixed points: stable node, unstable node, and saddle point, respectively.

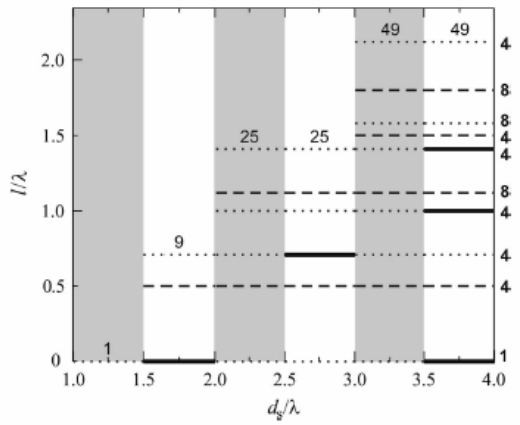


FIG. 5. Bifurcation of the spiral wave rotation under confined-domain feedback control. Number of fixed points inside the sensory domain is illustrated as a function of the normalized size of the domain, $d_s/\lambda$. Distance $l$ from the domain center of the fixed point is shown on the $y$ axis. Solid, dashed, and dotted bars indicate the fixed points: stable node, saddle point, and unstable node, respectively. Inserted numbers show the total number of fixed points for each range of $d_s$. Gray bands indicate the range where no stable rotating spirals exist.

that for the case $d_s=1.5\lambda$, we find a fourfold symmetric repetition of the pattern of Fig. 4(a). The stability of the four fixed points is lost when enlarging the domain size by about $0.5\lambda$, as shown in Fig. 4(c) for $d_s=3.0\lambda$. Here, all the fixed points that are stable in Fig. 4(b) become unstable.

The number of fixed points inside the square domain is 9, 25, and 49 for the side lengths $d_s=1.5\lambda$, $2.5\lambda$, and $3.0\lambda$ in Figs. 4(a)–4(c), respectively. Note that for domains smaller than $1.5\lambda$, there exists only one unstable fixed point, which is located at the center of the domain, as shown in Figs. 2(a)–2(c) and Fig. 3(a). However, the domain should not be too small—i.e., smaller than the spiral core. Because if such a small domain is located inside the core, there will be no modulation of the signal and consequently no feedback.

The total number of fixed points, $F_n$, can be described as a function of the the size of the domain $d_s$ according to $F_n=(2n+1)^2$, where $n=[d_s/\lambda-(d_s/\lambda \bmod 1)]$. For example, if $d_s=1.5\lambda$, then $n=1$ and therefore $F_n=9$, as shown in Fig. 4(a). Furthermore, the number of each type of fixed point is expressed as (i) number of stable nodes, $F_{sn}=n^2$, (ii) number of saddle points, $F_{sdn}=2n(n+1)$, and (iii) number of unstable nodes, $F_{un}=(n+1)^2$. One can see clearly that $F_n=F_{sn}+F_{sdn}+F_{un}$. Note that these relationships can be used for $d_s \geqslant 1.5\lambda$. For $d_s<1.5\lambda$, $F_n=F_{un}=1$ as mentioned above.

A bifurcation diagram characterizing the stability of the spiral core drift under a square-domain feedback control is shown in Fig. 5. Stable fixed points exist along the the solid bars in this diagram, whereas the shaded bands indicate the ranges of $d_s/\lambda$ in which no stable fixed point can be observed. Instead the spiral core moves asymptotically on closed attractive orbits, as previously illustrated for the trajectories evolving from unstable fixed points in Fig. 2 [except for Fig. 2(g) and the small attractor in the middle of Fig. 2(d)]. These properties of these orbits have some analogy to limit cycles in phase space. The number of fixed points increases stepwise with increasing domain size. Focusing on the stable fixed points (solid bars), their number increases as 1, 4, 9,…, corresponding to the relation $F_{sn}=n^2$ mentioned above. In addition, the stability of the fixed points changes also with enlarging the domain. For example, consider the stability of the fixed point located at the center of the domain (distance $l=0$): the dynamics of this point is unstable for $d_s/\lambda<1.5$ and becomes stable for $1.5 \leqslant d_s/\lambda<2.0$. For $d_s/\lambda \geqslant 2.0$ it is unstable until $d_s/\lambda \geqslant 3.5$. Note that the saddle points (dashed bars) keep their characteristics with increasing $d_s$.

## V. CONCLUSIONS

Our results demonstrate that the dynamics of the spiral waves under nonlocal feedback control depends sensitively on the geometry, shape and size of the sensory domain, from which the feedback signal is derived. The results in Fig. 1 show that the geometry of the sensory domain is reflected in the shape of the spiral tip trajectory. For a fixed domain shape—e.g., a square—a small increase of the domain size results in a decrease of the trajectory size as seen when comparing Fig. 2(b) with 2(c) and Fig. 2(f) with 2(g). Several shapes of the trajectory can be observed by enlarging the domain. Along the axis of increment of the domain size, the dynamics can be divided into two types, stable and unstable rotation, as shown in Figs. 2 and 5.

An explanation of the numerically observed effects is proposed by using flow maps constructed from the analysis of the feedback signal. The flow maps in Fig. 3 reveal that our feedback forcing leads to the existence of a discrete set of stable square-shaped orbits, which appear to be attractors for the spiral core drift. In addition, the flow maps demonstrate that the local and global dynamics of the spiral wave can be drastically changed by switching the sign of the feedback gain [see Figs. 3(a) and 3(b)]. It is shown that the shape and size of the trajectories of the spiral wave tip, as well as the stability of the spiral rotation, can be changed by varying the size or shape of the sensory domain. We suggest that the feedback method introduced in this work offers an efficient tool for controlling the dynamics of excitable media in biology [15–17].

## ACKNOWLEDGMENTS

O.K., S.K., and P.W. thank the Postgraduate Education and Research Program in Chemistry funded by the Royal Thai Government and O.K. thanks the Thailand Research Fund for financial support.

[1] *Handbook of Chaos Control*, edited by H.G. Schuster (Wiley-VCH, Weinheim, 1999).
[2] E. Ott, C. Grebogi, and J.A. Yorke, Phys. Rev. Lett. **64**, 1196 (1990).
[3] S. Jakubith, H.H. Rotermund, W. Engel, A. von Oertzen, and G. Ertl, Phys. Rev. Lett. **65**, 3013 (1990).
[4] J. Wolff, A.G. Papathanasiou, L.G. Kevrekidis, H.H. Rotermund, and G. Ertl, Science **294**, 134 (2001).
[5] Th. Pierre, G. Bonhomme, and A. Atipo, Phys. Rev. Lett. **76**, 2290 (1996).
[6] K. Krischer, J. Electroanal. Chem. **501**, 1 (2001).
[7] G. Franceschini, S. Bose, and E. Schöll, Phys. Rev. E **60**, 5426 (1999).
[8] T. Sakurai, E. Mihaliuk, F. Chirila, and K. Showalter, Science **296**, 2009 (2002).
[9] O.-U. Kheowan, C.K. Chan, V.S. Zykov, O. Rangsiman, and S.C. Müller, Phys. Rev. E **64**, 035201(R) (2001).
[10] O.-U. Kheowan, V.S. Zykov, and S.C. Müller, Phys. Chem. Chem. Phys. **4**, 1334 (2002).
[11] V.S. Zykov, G. Bordiougov, H. Brandtstädter, I. Gerdes, and H. Engel, Phys. Rev. Lett. **92**, 018304 (2004).
[12] O.-U. Kheowan, S. Kantrasiri, C. Uthaisar, V. Gáspár, and S.C. Müller, Chem. Phys. Lett. **389**, 140 (2004).
[13] A.T. Winfree, Science **175**, 634 (1972).
[14] S.C. Müller, T. Plesser, and B. Hess, Science **230**, 661 (1985).
[15] J.M. Davidenko, A.V. Pertsov, R. Salomonsz, W. Baxter, and J. Jalife, Nature (London) **355**, 349 (1992).
[16] M. Dahlem and S.C. Müller, Exp. Brain Res. **115**, 319 (1997).
[17] M. Falcke, Y. Li, J.D. Lechleiter, and P. Camacho, Biophys. J. **85**, 1474 (2003).
[18] B.J. Gluckman, H. Nguyen, S.L. Weinstein, and S.J. Schiff, J. Neurobiol. **21**, 590 (2001).
[19] R.J. Field and R.M. Noyes, J. Chem. Phys. **60**, 1877 (1974).
[20] W. Jahnke and A.T. Winfree, Int. J. Bifurcation Chaos **1**, 445 (1991).
[21] H.J. Krug, L. Pohlmann, and L. Kuhnert, J. Phys. Chem. **94**, 4862 (1990).
[22] V.S. Zykov, A.S. Mikhailov, and S.C. Müller, Phys. Rev. Lett. **78**, 3398 (1997).
[23] V.S. Zykov and S.C. Müller, Physica D **97**, 322 (1996).

Available online at www.sciencedirect.com
SCIENCE DIRECT®
Chemical Physics Letters 399 (2004) 506–511
CHEMICAL PHYSICS LETTERS
www.elsevier.com/locate/cplett

# Hypocycloidal resonance attractor for rigidly rotating spiral waves

On-Uma Kheowan [a,*], Chananate Uthaisar [a], Supichai Kantrasiri [a], Stefan C. Müller [b]

[a] Department of Chemistry, Mahidol University, Rama 6 Road, Bangkok 10400, Thailand
[b] Institut für Experimentelle Physik, Otto-von-Guericke-Universität, Universitätsplatz 2, D-39106 Magdeburg, Germany

Received 7 September 2004; in final form 12 October 2004

**Abstract**

Rigidly rotating spiral waves are investigated in the light sensitive excitable Belousov–Zhabotinsky reaction under local feedback control. Each light pulse is applied at a moment that corresponds to the passage of the wave front through a particular measuring point. For a small distance between the measuring point and the initial location of the spiral core, a resonance attractor with hypocycloidal shape is observed, whereas for a larger distance an epicycloidal resonance attractor occurs. The size of the attractor can be changed by introducing a time delay. Experimental and numerical results are compared with an earlier developed theory on the resonance attractor.


Controlling the dynamics of spiral waves is important for many excitable media including chemical systems like the Belousov–Zhabotinsky (BZ) reaction [1–6], or biological systems like cardiac tissue [7–10]. One effective control method is a local feedback algorithm. It has been suggested that this method can be applied to eliminate spiral waves in cardiac tissue [8], i.e., if certain properties of the medium are varied with the period of rotation of a spiral wave, the spiral wave will be subjected to a drift and can be eliminated at the boundary of the medium. Such a local feedback has been realized in the laboratory by disturbing spiral waves in the light-sensitive version of the BZ reaction [11] with a sequence of short light pulses [12–18]. Each stimulus was applied at an instant corresponding to the passage of the wave front through a particular measuring point. This local feedback mechanism was investigated originally for spirals with a 'meandering' tip describing a hypocycloidal trajectory that is characterized by two rotation periods: $T_0$, as measured at the center of the trajectory and $T_\infty$, as determined far away from it [14].

Under this feedback control two dynamical regimes, called entrainment attractor and resonance attractor, have been observed [14]. The entrainment attractor occurs if the measuring point is located close to the center of the unperturbed trajectory (initial distance $R_0$ about 1/3 of the spiral wavelength [14,15]). The period of external modulation becomes $T_m \approx T_0$, and the tip moves on a hypocycloid in perfect synchrony with the external signal. For larger $R_0$, the tip is found to move on the resonance attractor. At this larger distance, the average period of the triggered external stimuli is close to $T_\infty$, and no strict synchronization as in the case of the entrainment attractor is obtained. Both regimes are stable with respect to a small shift of the measuring point, which always constitutes the symmetry center of these attractor orbits [14].

More recently, this kind of local feedback control was also applied to rigidly rotating spiral waves [16–18], characterized by only one rotation period. In this case, only the resonance attractor was observed and mostly the trajectories of this attractor are epicycloids, i.e., their petals are directed inwards. However, it was reported in a numerical study [16] that very small resonance attractors may assume a hypocycloidal shape, i.e., with

* Corresponding author. Fax: +66 2 3547151.
*E-mail address:* scokw@mucc.mahidol.ac.th (O.-U. Kheowan).

0009-2614/$ - see front matter © 2004 Elsevier B.V. All rights reserved.
doi:10.1016/j.cplett.2004.10.046

outward directed petals. This latter case has not yet been investigated in the laboratory, and we show in this Letter that, in fact, hypocycloidal resonance attractors exist for rigidly rotating spiral waves and that their occurrence depends sensitively on the initial conditions chosen for the feedback signal. We investigate their dynamical features under the application of time delays. The results are corroborated by numerical simulations and compared with theoretical predictions.

The reaction was carried out in a petri dish (diameter, 5.5 cm) containing a thin layer (thickness, 0.30 mm) of silica gel [17]. The light sensitive $Ru(bpy)_3^{2+}$ catalyst was immobilized in the gel at a concentration of 4.2 mM. The BZ solution without catalyst was poured on top of the gel. After several minutes an equilibrium between liquid and gel was established and the following concentrations of reactants were reached: 0.20 M $NaBrO_3$, 0.17 M malonic acid, 0.39 M $H_2SO_4$, and 0.09 M NaBr. The gel and the solution were kept at a constant temperature of $25 \pm 1$ °C.

A wave front was broken with a spot (diameter, 1 cm) of intense light from a cold light source. As a consequence, the open ends of the wave begin to form a pair of spirals. One spiral was suppressed with the light spot to leave a single spiral in the center of the dish. This procedure defined the initial condition for all of the experiments. The gel in the petri dish was illuminated from below with a video projector and controlled by a computer. The pictures of the appearing oxidation waves were observed in transmitted light ($\lambda = 485$ nm), detected by a CCD camera and stored with a computer program. The spiral rotation was characterized by considering the trajectory of the spiral tip detected with image processing techniques, as specified in [3,14,17].

For a given background light intensity $I_0 = 0.061 \pm 0.001$ mW/cm$^2$, the spiral tip rotates rigidly around a closed circle with a diameter of $0.36 \pm 0.03$ mm. The unperturbed rotation period is $T_u = 39.41 \pm 2.14$ s and the spiral wavelength is $\lambda = 1.92 \pm 0.10$ mm. The rigid rotation is disturbed by a sequence of short light pulses (amplitude $A$, duration 5 s), applied at the moment, when the wave front passes through a preselected measuring point, or after some time delay $\tau$. During the pulse the total light intensity $I$ is either increased (positive pulse, $I > I_0$) or decreased (negative pulse, $I < I_0$).

The hypocycloidal resonance attractor is found to occur if the measuring point is located very close to the core center of the unperturbed spiral (Fig. 1a), i.e. $R_0 \leqslant 15\lambda$. In this example the spiral wave tip asymptotically approaches a five-lobed hypocycloidal trajectory with its symmetry center coinciding with the measuring point (Fig. 1b). The ratio of the rotation period at the measuring point ($T_{mp}$) to the unperturbed period, $T_{mp}/T_u$, is 0.867 and the ratio of the attractor radius to the spiral wavelength, $R_s/\lambda$ is 0.117. The light pulses

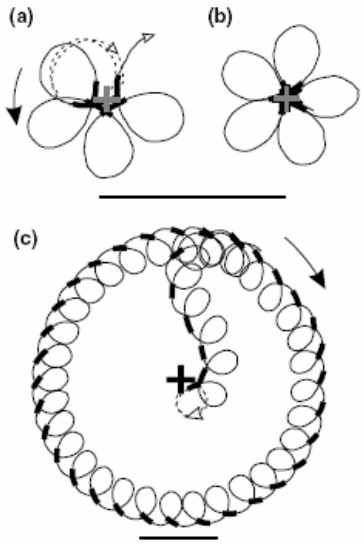


Fig. 1. Hypocycloidal (a–b) and epicycloidal (c) resonance attractors of the rigidly rotating spiral. Initial distance between measuring point (cross) and unperturbed core center, $R_0$: (a–b) $0.093\lambda$ and (c) $0.155\lambda$. $I_0 = 0.061$ mW/cm$^2$; $A = 0.050$ mW/cm$^2$. (a) Transient state of trajectory in (b), which is the stationary attractor several sprial rotations after starting the feedback. Thick segments indicate application of light pulses. The dotted line depicts the unperturbed spiral tip trajectory. Open and filled arrows indicate the rotation direction of the sprial tip and the spiral core, resp. The radius of an attractor $R_s$ is defined as the average of inner and outer radius of the looping trajectory. Scale bar: 1 mm.

appear in the inner part of the loopy trajectory, and the drift direction of the spiral core is opposite to that of the tip rotation.

For $R_0 > 0.15\lambda$, the spiral tip describes an epicycloidal orbit centered at the measuring point, and we find $T_{mp}/T_u = 1.098$, $R_s/\lambda = 0.805$. The light pulses occur when the tip moves along the outer part of the loopy trajectory. The sense of rotation is the same for the spiral core and the spiral tip.

The dynamics of the hypocycloidal attractor was further studied after introducing a time delay $\tau$ into the feedback loop. Examples for positive ($A = 0.040$ mW/cm$^2$) and negative pulse feedback ($A = -0.031$ mW/cm$^2$) are shown in Fig. 2. Starting with $\tau = 0$ in Fig. 2a, the radius of the hypocycloidal resonance attractor increases with $\tau$. This growth is accompanied by an increase of the number of lobes in the trajectory, i.e., 5, 6, and 7 lobes for $\tau/T_u = 0$, 0.026, 0.053, respectively. If the delay reaches a certain value ($\tau/T_u = 0.067$), a transition from the hypo- to the epicycloidal regime takes place. In the range $0.067 \leqslant \tau/T_u \leqslant 0.679$ only this regime is observed, although a very small $R_0$ was chosen. Note that the radius of the epicycloidal attractor decreases with $\tau$ in agreement with previous findings [16,17]. At $\tau/T_u = 0.679$, however, this radius becomes so small, that the measuring point is finally located inside the spiral core and no light pulse is triggered any more. Then a further increase of $\tau$ brings the

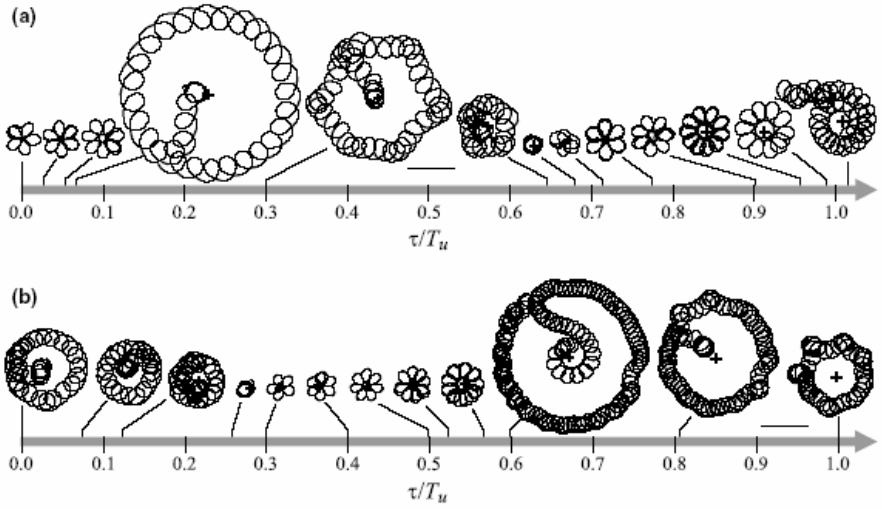


Fig. 2. Trajectories of the spiral tip under variation of the time delay τ: (a) positive pulse feedback with amplitude $A = 0.043$ mW/cm$^2$; (b) negative pulse feedback with $A = -0.031$ mW/cm$^2$, where $I_o = 0.061$ mW/cm$^2$. The measuring point (crosses) was initially placed close to the unperturbed spiral core ($R_0 \leqslant 0.15\lambda$), except for the two orbits in (b) at $T_{mp}/T_u = 0.805$ and 1. Thick segments correspond to the application of light pulses. Scale bar: 1 mm.

dynamics of the system back to the hypocycloidal regime, where the size of the attractor orbits increases with τ ($0.775 \leqslant \tau/T_u \leqslant 0.989$). Hypocycloidal attractor becomes again unstable at $\tau/T_u = 1.038$, consequently the dynamics switches, once more, to the epicycloidal regime.

Examples of hypocycloidal resonance attractors observed for negative pulse feedback are shown in Fig. 2b in the range $0.3 \leqslant \tau/T_u \leqslant 0.56$. Here, the pulses (indicated by thick segments) occur in the outer part of the hypocycloidal trajectory in contrast with the finding for positive pulse feedback (see Figs. 1a and 2a), where the pulses appear in the inner part. However, the time delay plays a similar role here, i.e., the radius of the attractor increases with τ.

Further instabilities of the hypocycloidal attractors are observed, when a prolonged time delay ($\tau/T_u > 1$) is introduced (Fig. 3). A clear deviation from a circular symmetric attractor appears for $\tau/T_u = 2$ (extended hypocycloid, Fig. 3c). With increasing τ deviations become more pronounced: Apparently, the trajectories in Fig. 3d–f share a similar feature: they consist of a 'head' (circular, outward loops), and a 'tail' (extended, inward loops). The length of the tail increases with τ.

The dependence of the attractor radius $R_s$ on the time delay τ is summarized in Fig. 4. The characteristics of the epicycloidal resonance attractors shown in this graph (diamonds and crosses) agree well with previous studies [16,17]. The new results for the hypocycloidal resonance attractor are represented by squares and triangles (see caption).

A theoretical analysis has previously shown [16] that several stationary solutions of the attractor radius $R_s$

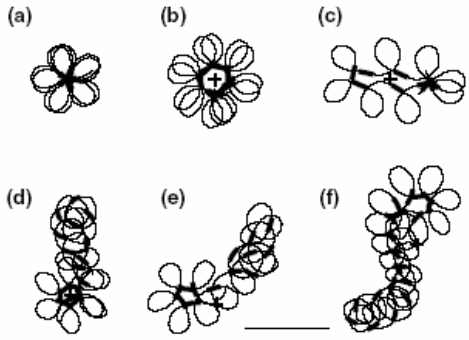


Fig. 3. Trajectories of the spiral wave tip observed for large time delays τ, where $I_0 = 0.062$ mW/cm$^2$, $A = 0.091$ mW/cm$^2$: (a) $\tau/T_u = 0$; (b) $\tau/T_u = 1$; (c) $\tau/T_u = 2$; (d) $\tau/T_u = 3$; (e) $\tau/T_u = 4$; (f) $\tau/T_u = 6$. Thick segments correspond to the application of light pulses. Scale bar: 1 mm.

exist for each value of the time delay τ and that the following equations should be satisfied:

$$\frac{\tau}{T_u} = \frac{\Theta(R_s) - \arccos(h/(2R_s)) - \psi}{2\pi} + m, \tag{1}$$

$$\frac{\tau}{T_u} = \frac{\Theta(R_s) + \arccos(h/(2R_s)) - \psi}{2\pi} + m, \tag{2}$$

where $m$ is a positive integer. The function $\Theta(r)$ (see inset of Fig. 4) and the values $h$ and $\psi$ are measured quantities (cf. [17]). The size of the resonance orbit can then be predicted at any time delay τ by substituting these data into Eqs. (1) and (2). Linear stability analysis shows that Eq. (1) describes stable orbits and Eq. (2) unstable ones [16]. The computed results are shown in

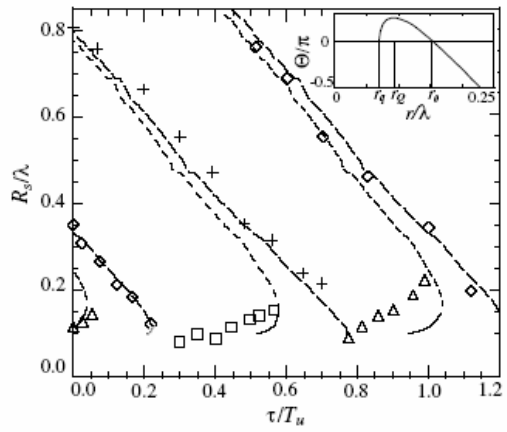


Fig. 4. Attractor radius $R_s$ for different delay times $\tau$: diamonds and crosses, epicycloidal attractors with negative ($A = -0.030$ mW/cm$^2$) and positive pulse ($A = 0.051$ mW/cm$^2$); triangles and squares, hypocycloidal attractors with positive ($A = 0.041$ mW/cm$^2$) and negative pulse ($A = -0.031$ mW/cm$^2$), where $I_0 = 0.061$ mW/cm$^2$. Solid and short-dashed curves are prediction of $R_s(\tau)$ from Eqs. (1) and (2) for stable and unstable hypocycloidal attractors, resp, with $h_n = 0.215 \pm 0.003$ mm, $\psi_n = 4.00 \pm 0.11$ rad for negative, and $h_p = 0.328 \pm 0.005$ mm, $\psi_p = 0.91 \pm 0.07$ rad for positive pulse. Similarly, long-dashed and dotted curves are prediction of $R_s(\tau)$ for stable and unstable epicycloidal attractors, resp. *Inset:* function $\Theta(r)$ specifying the experimentally observed shape of the spiral wave front. $\Theta(r)$ increases with $r$ in the vicinity of the core radius $r_q$, reaches a maximum at $r = r_Q$, and becomes negative for $r > r_0$.

Fig. 4, where each branch of the dependency $R_s$ was obtained for a fixed value of $m$.

In this figure there are mostly long-dashed branches and mostly short-dashed branches. The mostly short-dashed curves were computed from Eq. (2), with a positive sign in front of $\arccos(h/(2R_s))$. Since the change of slope of the $\Theta(r)$ curve in the interval from $r_q$ to $r_0$ implies a switching of stability [16], there is an unstable portion of these curves (short-dashed) and a stable one (solid). Consider the shortest branch close to the ordinate of Fig. 4 ($\tau/T_u \leqslant 0.05$). Our experimental results suggest that with positive pulses there exist only hypocycloidal attractors in this interval, whereas epicycloidal ones will not be stable. In a similar manner, the existence of other sets of hypocycloidal resonance attractors observed in experiments (all squares and triangles in Fig. 4) can be explained with other branches computed according to Eq. (2). Note that there are very small unstable branches (e.g., dotted arc-shaped segment at $\tau/T_u \approx 0.2$) connected to the lower end of each stable branch of epicycloidal resonance attractors, as reported earlier [16].

Some of these results were complemented by numerical simulations using Oregonator model [19,20] extended by a term $\phi = \phi(t)$ that accounts for the effect of bromide ions produced by the illumination [21]:

$$\frac{\partial u}{\partial t} = \frac{1}{\varepsilon}\left[u - u^2 - (fv + \phi)\frac{u - q}{u + q}\right] + D_u \nabla^2 u, \tag{3}$$

$$\frac{\partial u}{\partial t} = u - v. \tag{4}$$

Here, the variables $u$ and $v$ correspond to the concentration of the autocatalytic species $HBrO_2$ and the oxidized form of the catalyst, respectively. Due to the immobilization of the catalyst, variable $v$ does not diffuse in this model. The parameters $\varepsilon = 0.05$, $q = 0.002$, $f = 3.5$ and $D_u = 1$ are kept constant.

A series of trajectories of the spiral wave tip simulated under local feedback control is shown in Fig. 5a. These simulation results are consistent with the epi- and hypocycloidal resonance attractors observed experimentally (see Fig. 2a). A numerical study of the dependence of their radius $R_s$ on $\tau$, as shown in Fig. 5b, is in good agreement with the theoretical predictions. There is, however, some discrepancy with the experimental findings (see Fig. 4). In the experiments hypocycloidal resonance attractors are observed in a quite extended range of delay times, whereas the corresponding intervals in theory and simulations are comparatively narrow. This disagreement becomes more pronounced as $\tau$ increases. A possible reason for this is the relaxation and delayed response of the spiral wave in experiments following the application of a light pulse [22].

Our experimental results show that there are two types of resonance attractors that can be observed for a rigidly rotating spiral wave under local feedback control: an epi- and a hypocycloidal one. Type, size and stability of the attractor can be changed by introducing a time delay into the feedback loop. In Table 1 some of the characteristic properties are compared with each other.

Tip trajectories corresponding to near-resonance conditions of the two attractors remind one of the resonance drift induced by periodic external forcing of rigidly rotating spiral waves [23]. If $T_{mp}$ and $T_u$ are exactly equal, the perfect resonance is expected, with the core center moving along a straight line. But the period of modulation induced by the local feedback mechanism is just near-resonance, i.e., either $T_{mp} > T_u$ or $T_{mp} < T_u$, therefore the trajectory has either epi- or hypocycloidal shape.

A control parameter that defines the boundary between the two types of attractors is the initial distance $R_0$ between measuring point and core center. In fact, the hypocycloidal shape is observed for $R_0 < 0.15\lambda$, whereas for larger values of $R_0$ only the epicycloidal one appears to be realized. On the other hand, $R_0$ must not be too small, i.e., it must be larger than the core radius, $r_q$. Otherwise, with the measuring point located inside the core no light pulse is triggered. According to [16] the hypocycloidal resonance attractor is reached for the interval $r_q < R_0 < r_0$. In our experiments $r_q = 0.070\lambda$ and

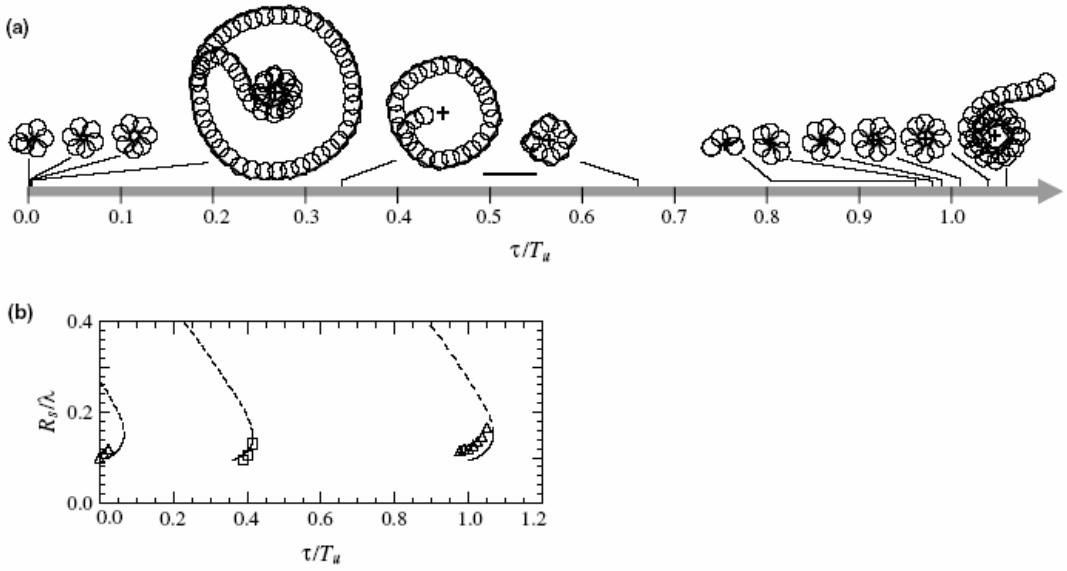


Fig. 5. (a) Simulation of epi- and hypocycloidal attractors computed from Eqs. (3) and (4) for positive pulse ($A = 0.0035$, duration = $12.19T_u$) under variation of $\tau$. The measuring point (crosses) was initially placed close to the unperturbed spiral core. Thick segments correspond to the application of the light pulses. Scale bar: 20 s.u. (b) Attractor radius $R_s$ for different $\tau$: triangles, attractors with positive pulse; squares, attractors with negative pulse ($A = -0.0020$, duration = $12.19T_u$), with background value $\phi_0 = 0.01$. Solid and dashed curves: $R_s(\tau)$ for stable and unstable solutions, resp, computed from Eq. (2) with: $h_n = 0.097\lambda$, $\psi_p = 5.026$ for a negative pulse; $h_p = 0.128\lambda$, $\psi_p = 0.848$ for a positive pulse.

Table 1
Properties of the epi- and hypocycloidal resonance attractor

| Characteristic property | Epicycloidal attractor | Hypocycloidal attractor |
|---|---|---|
| Rotation direction of tip and core | Coincide | Opposite |
| Rotation period, $T_{mp}$ | $>T_u$ | $>T_u$ |
| Attractor size | Large | Small |
| Pulse interval location | Outer part of the trajectory | Inner part of the trajectory |
| Effect of increasing $\tau$ | Attractor radius decreases | Attractor radius increases |

$r_0 = 0.152\lambda$ (see inset of Fig. 4). Hence, the boundary value $R_0 < 0.15\lambda$ is in good agreement with theoretical expectations [16].

Interestingly, most of the properties of the hypocycloidal resonance attractor shown in Table 1, which refer to the rigidly rotating spiral waves, are very similar to those of the entrainment attractor for meandering spirals [14,15], although the dynamics of the rigidly rotating and meandering spirals differ significantly by the fact that their movement is composed of either one (spatially uniform) or two (not spatially uniform) rotation frequencies.

To be noticed is the difference in the modulation period. For rigid rotation it is equivalent to the rotation period at the measuring point $T_{mp}$, where $T_{mp} < T_u$ for the hypocycloidal resonance attractor. On the other hand, for the entrainment attractor of meandering spirals, it is equal or very close to the period $T_0$ at the center of the unperturbed hypocycloidal trajectory. Finally, we point to our observation that the attractor shapes deviate strongly from circular symmetry, if the time delay in the feedback loop becomes relatively long. To study further instabilities of the resonance attractor for such long delays is an interesting challenge for future work.

## Acknowledgements

O.K., S.K. and C.U. thank the Postgraduate Education and Research Program in Chemistry funded by the Royal Thai Government and O.K. thanks the Thailand Research Fund for financial support.

## References

[1] A.T. Winfree, Science 175 (1972) 634.
[2] S.C. Müller, T. Plesser, B. Hess, Science 230 (1985) 661.
[3] O. Steinbock, V.S. Zykov, S.C. Müller, Nature 366 (1993) 322.
[4] V.K. Vanag, L. Yang, M. Dolnik, A.M. Zhabotinsky, I.R. Epstein, Nature 406 (2000) 389.

[5] A.L. Lin, M. Bertram, K. Martinez, H.L. Swinney, Phys. Rev. Lett. 84 (2000) 4240.
[6] T. Sakurai, E. Mihaliuk, F. Chirila, K. Showalter, Science 296 (2002) 2009.
[7] J.M. Davidenko, A.V. Pertsov, R. Solomonsz, W. Baxter, J. Jalife, Nature (London) 355 (1992) 349.
[8] A.V. Panfilov, S.C. Müller, V.S. Zykov, J.P. Keener, Phys. Rev. E 61 (2000) 4644.
[9] F. Xie, Z. Qu, A. Garfinkel, J.N. Weiss, Am. J. Physiol. Heart Circ. Physiol. 280 (2001) 1667.
[10] K.H.W.J. Ten Tusscher, D. Noble, P.J. Noble, A.V. Panfilov, Am. J. Physiol. Heart Circ. Physiol. 286 (2004) 1573.
[11] L. Kuhnert, Naturwissenschaften 73 (1986) 96.
[12] K.I. Agladze, V.A. Davydov, A.S. Mikhailov, JETP Lett. 45 (1987) 767.
[13] M. Braune, H. Engel, Chem. Phys. Lett. 211 (1993) 534.
[14] S. Grill, V.S. Zykov, S.C. Müller, Phys. Rev. Lett. 75 (1995) 3368.
[15] S. Grill, V.S. Zykov, S.C. Müller, J. Phys. Chem. 100 (1996) 19082.
[16] A. Karma, V.S. Zykov, Phys. Rev. Lett. 83 (1999) 2453.
[17] O.-U. Kheowan, V.S. Zykov, O. Rangsiman, S.C. Müller, Phys. Rev. Lett. 86 (2001) 2170.
[18] V.S. Zykov, O.-U. Kheowan, O. Rangsiman, S.C. Müller, Phys. Rev. E 65 (2002) 26206.
[19] R.J. Field, R.M. Noyes, J. Chem. Phys. 60 (1974) 1877.
[20] W. Jahnke, A.T. Winfree, Int. J. Bifur. Chaos 1 (1991) 445.
[21] H.J. Krug, L. Pohlmann, L. Kuhnert, J. Phys. Chem. 94 (1990) 4862.
[22] M.K. Ram Reddy, M. Dahlem, V.S. Zykov, S.C. Müller, Chem. Phys. Lett. 236 (1995) 111.
[23] V.A. Davydov, V.S. Zykov, A.S. Mikhailov, Sov. Phys. Uspekhi 34 (1991) 665.